

Spatial-dispersion-induced birefringence in metamaterials with cubic symmetryAlexander V. Chebykin,¹ Maxim A. Gorlach,^{1,2,*} and Pavel A. Belov¹¹*ITMO University, St. Petersburg 197101, Russia*²*Belarusian State University, Minsk 220030, Belarus*

(Received 21 April 2015; revised manuscript received 12 July 2015; published 28 July 2015)

We consider an array of isotropic particles possessing electric polarizability located in the sites of a cubic lattice. The dispersion properties of the structure and the polarization of eigenmodes are studied employing the discrete dipole model. We reveal the features beyond the effective medium model, namely, the anisotropy of the structure induced by spatial dispersion, and suggest a simple experiment allowing one to observe the effect. Additionally, we demonstrate that the eigenmodes of the structure are neither transverse nor longitudinal but have a “mixed” polarization state in the general case.

DOI: [10.1103/PhysRevB.92.045127](https://doi.org/10.1103/PhysRevB.92.045127)

PACS number(s): 42.25.Lc, 42.70.Qs, 78.20.Fm

I. INTRODUCTION

The modern condensed matter physics deals with various many-particle systems with complicated interactions between the constituent elements. For that reason, the approximate models that are capable of capturing the main features of the system neglecting some minor effects are of particular relevance. The technologies existing currently allow one to create and investigate such artificial structures as optical lattices, formed by cold atoms [1], regular arrays of quantum dots in semiconductor physics [2], and arrays of scatterers [3–5] in metamaterial physics. Tailoring the properties of metaatoms as well as the geometry of their arrangement in the lattice, it is possible to fabricate metamaterial with unusual and to some extent exotic electromagnetic response.

It is well established that there exists a class of metamaterials exhibiting strong spatial dispersion effects that do not occur in natural structures [6,7]. Moreover, it is known that the nonlocal effects can be either suppressed or enhanced depending on the geometry of metamaterial [8] and operation regime [5]. Thus, the possibility to tailor spatially dispersive response of metamaterial provides a novel degree of freedom in material science and challenges metamaterial engineers.

In the present paper, we consider electromagnetic properties of metamaterial composed of isotropic particles (namely, plasmonic spheres) located in the sites of a cubic lattice (Fig. 1). Such a structure is described by the isotropic permittivity tensor from the standpoint of the local effective medium model [9]. Additionally, this kind of metamaterial was investigated previously in many works [4,10–15]. We revisit the problem paying special attention to the nonlocal effects in the structure. It should be mentioned that many authors studied the propagation of the wave along the crystal axes without paying attention to any other directions of propagation [13–15] or investigated particular eigenmode polarization along the crystal axis [16]. It seems to be quite natural because this assumption leads to the simplification of equations describing wave propagation whereas any medium formed by isotropic particles in the sites of a cubic lattice is fully isotropic in the effective medium model validity domain [9]. However, this isotropy is destroyed by spatial dispersion effects as the

direction of wave vector \vec{k} with respect to the crystallographic axes provides a selected direction in space. This simple observation was pointed out in a number of works [17,18] and is termed as spatial-dispersion-induced birefringence. This effect was observed experimentally for such natural materials as Cu_2O , [19,20] CaF_2 , and BaF_2 [21,22] but expectedly was sufficiently weak. All the previous theoretical studies of this effect [17,18] relied on the expansions of the tensor $\hat{\epsilon}(\omega, \vec{k})$ with respect to \vec{k} up to the second order employing further some symmetry considerations. In our work, we use the nonlocal homogenization approach [23] employing the discrete dipole model [10,24–26]. This theoretical approach, as it was demonstrated in the previous publications [3–5,7,27] allows one to provide the self-consistent description of spatial dispersion effects in the structure without perturbative expansions with respect to wave vector. We demonstrate that the eigenmodes of the structure are neither purely transverse nor purely longitudinal in the general case. We also propose a scheme of experiment involving the measurements of the reflection coefficients for different polarizations allowing one to observe spatial-dispersion-induced birefringence in metamaterials. The theoretical conclusions are verified by numerical simulations.¹

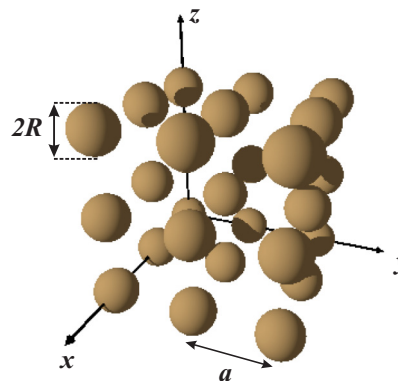
¹Software package CST MICROWAVE STUDIO.

FIG. 1. (Color online) Metamaterial composed of isotropic particles arranged in the sites of a cubic lattice.

*maxim.gorlach.blr@gmail.com

The rest of the paper is organized as follows. In Sec. II, the homogenization of the discrete structure is outlined and the dispersion equation is provided. Section III contains the calculated dispersion diagram and its discussion. The typical isofrequency contours and the information about the polarization of eigenmodes are provided in Sec. IV. In Sec. V, the scheme of experiment revealing spatial-dispersion-induced birefringence in metamaterials is discussed and the theoretical results are compared with the results of numerical simulations. Finally, Sec. VI contains the drawn conclusions. Some computational details regarding the discrete dipole model are moved to Appendixes A and B.

II. HOMOGENIZATION OF THE STRUCTURE AND DISPERSION PROPERTIES

The electromagnetic homogenization of metamaterial means the derivation of effective material parameters from the known properties of constituent elements and known interactions between them. For the structure consisting of electric scatterers, this procedure was discussed in Ref. [4]. In the case when the discrete dipole model can be applied, the derivation of the structure effective material parameters is briefly outlined below.

We use the CGS system of units and assume $e^{-i\omega t}$ time dependence of monochromatic fields; $q = \omega/c$ and \vec{k} is arbitrary wave vector. According to the general homogenization scheme [23] we consider excitation of the structure by the external distributed sources $\vec{j}(\vec{r}) = \vec{j}_0 e^{i\vec{k}\cdot\vec{r}}$. If placed in a vacuum, such sources create a monochromatic field $\vec{E}_e(\vec{r}) = \vec{E}_{e0} e^{i\vec{k}\cdot\vec{r}}$. Then the equation for the dipole moment of the scatterer in the coordinate origin is as follows [3,24,25]:

$$\vec{d} = \hat{\alpha} \left[\sum_{(m,n,l) \neq (0,0,0)} \hat{G}(-\vec{r}_{mnl}) \vec{d}_{mnl} + \vec{E}_{e0} \right], \quad (1)$$

where $\hat{\alpha} = \alpha \hat{I}$ is the polarizability tensor of the scatterer, m, n, l are the integers enumerating lattice sites, $\vec{r}_{mnl} = ma \vec{e}_x + na \vec{e}_y + la \vec{e}_z$, and a is the lattice period. The distribution of the scatterer dipole moments in space is determined by the external excitation and has the form $\vec{d}_{mnl} = \vec{d} e^{i\vec{k}\cdot\vec{r}_{mnl}}$. The external field can be related to the amplitude of the scatterers dipole moment using Eq. (1):

$$\vec{E}_{e0} = [\hat{\alpha}^{-1} - \hat{G}_{\vec{k}}] \vec{d}, \quad (2)$$

where the lattice sum,

$$\hat{G}_{\vec{k}}(q; \vec{k}) \equiv \sum_{(m,n,l) \neq (0,0,0)} \hat{G}(\vec{r}_{mnl}) e^{-i\vec{k}\cdot\vec{r}_{mnl}}, \quad (3)$$

is introduced.

Homogenization of the structure implies the derivation of the relation between the averaged electric field and the averaged polarization; the averaged fields are defined as follows [23,28]:

$$\begin{aligned} \langle \vec{E} \rangle &= \frac{1}{a^3} \int_{V_0} \vec{E}(\vec{r}) e^{-i\vec{k}\cdot\vec{r}} d^3\vec{r}, \\ \langle \vec{P} \rangle &= \frac{1}{a^3} \int_{V_0} \vec{P}(\vec{r}) e^{-i\vec{k}\cdot\vec{r}} d^3\vec{r} = \frac{\vec{d}}{a^3}. \end{aligned} \quad (4)$$

The total electric field in the structure can be represented as the sum of the external field $\vec{E}_e(\vec{r})$ and the field $\vec{E}_s(\vec{r})$ created by the dipoles of the polarized structure. The latter can be related to the averaged polarization of the structure via [28]

$$\langle \vec{E}_s \rangle = \hat{\Gamma}_{\vec{k}} \vec{d}, \quad \hat{\Gamma}_{\vec{k}} = -\frac{4\pi}{a^3} \frac{q^2 \hat{I} - \vec{k} \otimes \vec{k}}{q^2 - k^2}. \quad (5)$$

Combining Eqs. (2) and (5), we derive

$$\langle \vec{E} \rangle \equiv \langle \vec{E}_e \rangle + \langle \vec{E}_s \rangle = [\hat{\alpha}^{-1} - \hat{C}_{\vec{k}}] \vec{d}, \quad (6)$$

where the designation $\hat{C}_{\vec{k}} = \hat{G}_{\vec{k}} - \hat{\Gamma}_{\vec{k}}$ is employed. The quantity $\hat{C}_{\vec{k}}$ represents the interaction constant of the lattice and it is equal $4\pi/(3a^3) \hat{I}$ in the quasistatic limit $ka \ll 1$, $qa \ll 1$ [9,29]. Equation (6) establishes a link between the averaged structure polarization and the averaged field. Thus, the effective susceptibility of the structure is $\hat{\chi} = [\hat{\alpha}^{-1} - \hat{C}_{\vec{k}}]^{-1}/a^3$, and the effective nonlocal permittivity tensor is as follows [4,7]:

$$\hat{\varepsilon}(\omega, \vec{k}) = \hat{I} + \frac{4\pi}{a^3} [\hat{\alpha}^{-1}(\omega) - \hat{C}_{\vec{k}}(q; \vec{k})]^{-1}, \quad (7)$$

where $\hat{\alpha}$ and $\hat{C}_{\vec{k}}$ depend on frequency in the general case. Moreover, $\hat{C}_{\vec{k}}$ depends on the wave vector. We also note that in the lossless case the imaginary parts of $\hat{\alpha}^{-1}$ (corresponding to the radiation loss contribution) and $\hat{C}_{\vec{k}}$ cancel each other for the propagating modes [3], and the structure effective permittivity is a real valued function. If spatial dispersion effects are neglected and a quasistatic expression for the interaction constant is used, one obtains an isotropic permittivity tensor of the structure corresponding to the Clausius-Mossotti formula [9]:

$$\varepsilon(\omega, \vec{k}) = 1 + \frac{4\pi}{a^3} [\alpha^{-1}(\omega) - 4\pi/(3a^3)]^{-1}. \quad (8)$$

Substituting the derived effective permittivity Eq. (7) to the standard dispersion equation [30],

$$|\vec{k} \otimes \vec{k} - k^2 \hat{I} + q^2 \hat{\varepsilon}(\omega, \vec{k})| = 0, \quad (9)$$

it is easy to deduce the dispersion equation for the eigenmodes in the structure [10,15]:

$$|\hat{\alpha}^{-1} - \hat{G}_{\vec{k}}(q; \vec{k})| = 0. \quad (10)$$

This dispersion equation can be easily envisioned from Eq. (2) if one sets \vec{E}_{e0} to zero (no external excitation) and requires the system to have nontrivial solutions \vec{d} corresponding to the eigenmodes.

III. DISPERSION DIAGRAM ANALYSIS

We solve the dispersion equation Eq. (10) numerically using rapidly convergent expressions for matrix elements of the tensor $\hat{G}_{\vec{k}}$ given in Appendix A. Numerical calculations are performed for a model structure consisting of spherical isotropic particles with the radius $R = a/2.1$, permittivity of particle material $\varepsilon_p(\omega) = 1 - \omega_p^2/\omega^2$, where the plasma frequency $\omega_p = \omega_0 \sqrt{3} = 0.229 c/a$, and the resonance frequency of a single particle is $\omega_0 = 0.132 c/a$, the same as in Refs. [4,16]. The inverse polarizability of the individual

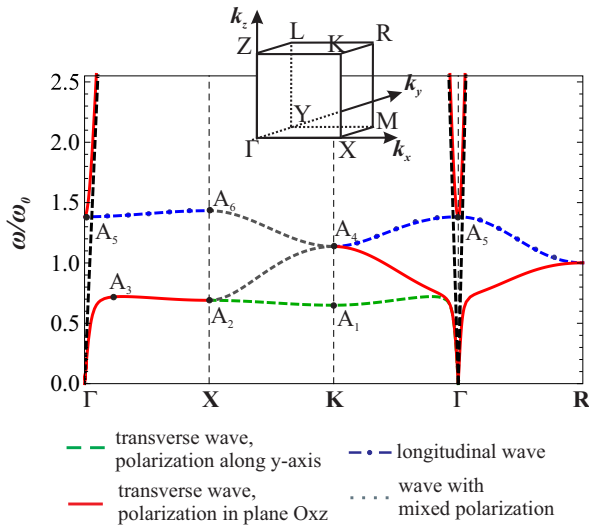


FIG. 2. (Color online) The dispersion diagram for the structure composed of isotropic particles with electric polarizability.

particle is set to

$$\alpha^{-1} = \alpha_0^{-1} - \frac{2iq^3}{3}, \quad \alpha_0 = \frac{\varepsilon_p - 1}{\varepsilon_p + 2} R^3. \quad (11)$$

The term $-2iq^3/3$ in the latter expression describes the radiation loss contribution [31].

The dispersion diagram is plotted in Fig. 2 for the directions of propagation ΓX , XK , $K\Gamma$, ΓR . It can be seen that the degeneracy of the transverse eigenmodes takes place for some directions of propagation, whereas for the other directions the degeneracy is removed. This degeneracy removal reflects the anisotropic properties acquired by the structure. To understand the most important features of the dispersion diagram in more detail, we analyze some particular cases when the dispersion equation simplifies considerably; we assume that the coordinate axes are aligned along the crystallographic axes of the structure.

For the waves propagating in the ΓX direction ($k_x \neq 0$, $k_y = k_z = 0$), $G_k^{xy}(q; k_x, 0, 0) = G_k^{xz}(q; k_x, 0, 0) = G_k^{yz}(q; k_x, 0, 0) = 0$ (see Appendix A). The dispersion Eq. (10) splits into three independent equations:

$$\begin{aligned} \alpha^{-1} - G_k^{zz}(q; k_x, 0, 0) &= 0, \\ \alpha^{-1} - G_k^{yy}(q; k_x, 0, 0) &= 0, \\ \alpha^{-1} - G_k^{xx}(q; k_x, 0, 0) &= 0. \end{aligned} \quad (12)$$

The first two relations in Eq. (12) describe the conventional transverse wave ($d_x = 0$); two equations account for two possible polarizations of the transverse wave. These equations are exactly the same as the dispersion equation for TM waves in the structure consisting of the uniaxial electric scatterers [3,5]. As $G_k^{yy}(q; k_x, 0, 0) = G_k^{zz}(q; k_x, 0, 0)$, the degeneracy of the transverse eigenmodes propagating in the ΓX direction is observed as for isotropic medium. The third equation in Eq. (12) describes the longitudinal wave polarized along its wave vector ($d_y = d_z = 0$). The longitudinal modes are known to arise in spatially dispersive structures [4,18].

For the waves propagating in the ΓR direction ($k_x = k_y = k_z$), $G_k^{xx}(q; k_x, k_x, k_x) = G_k^{yy}(q; k_x, k_x, k_x) = G_k^{zz}(q; k_x, k_x, k_x)$, and $G_k^{xy}(q; k_x, k_x, k_x) = G_k^{xz}(q; k_x, k_x, k_x) = G_k^{yz}(q; k_x, k_x, k_x)$. Therefore, the dispersion equation Eq. (10) simplifies to the following relations:

$$\begin{aligned} \alpha^{-1} - G_k^{xx} - G_k^{xy} &= 0, \\ \alpha^{-1} - G_k^{xx} - G_k^{xy} &= 0, \\ \alpha^{-1} - G_k^{xx} + 2G_k^{xy} &= 0. \end{aligned} \quad (13)$$

The eigenmode described by the first two relations of Eq. (13) is doubly degenerate and its polarization state is such that $d_x + d_y + d_z = 0$, or $\vec{d} \cdot \vec{k} = 0$, i.e., the wave is transverse. The eigenmode described by the third relation of Eq. (13) satisfies the formula $d_x = d_y = d_z$, i.e., it is polarized along the wave vector; this mode clearly corresponds to the longitudinal wave. If $k_x = \pi$, G_k^{xy} vanishes and all the equations, Eq. (13), coincide, i.e., all the dispersion curves touch each other at the edge of the Brillouin zone. Therefore, seven directions corresponding to edges and main diagonals of the cube in the Brillouin zone are the optical axes of the crystal. The same conclusion was drawn in Refs. [17,18] after the investigation of the second-order spatial dispersion corrections to the effective permittivity tensor employing symmetry considerations; in the present reasoning we do not employ any perturbative expansions with respect to \vec{k} .

Considering the directions of propagation different from the specified optical axes, we notice that the degeneracy of the transverse eigenmodes is removed in the general case of propagation. Thus, the structure acquires anisotropic properties induced by the spatial dispersion effects. Namely, the anisotropy arises for the waves propagating in the ΓK direction ($k_y = 0$, $k_x = k_z$). In this case, $G_k^{xy}(q; k_x, 0, k_x) = G_k^{yz}(q; k_x, 0, k_x) = 0$, and $G_k^{xx}(q; k_x, 0, k_x) = G_k^{zz}(q; k_x, 0, k_x)$. The dispersion equation Eq. (10) yields

$$\begin{aligned} \alpha^{-1} - G_k^{yy} &= 0, \\ \alpha^{-1} - G_k^{xx} + G_k^{xz} &= 0, \\ \alpha^{-1} - G_k^{xx} - G_k^{xz} &= 0. \end{aligned} \quad (14)$$

The first relation of Eq. (14) corresponds to the transverse wave polarized along the y axis, i.e., $d_x = d_z = 0$, $d_y \neq 0$. The second relation of Eq. (14) satisfies the conditions $d_y = 0$, and $d_x + d_z = 0$, i.e., $\vec{d} \cdot \vec{k} = 0$. Therefore, it describes the transverse mode. However, the dispersion equations for transverse modes do not coincide that means the anisotropy of the structure. As it is proved in Sec. II, this anisotropy cannot be captured by the local effective medium model and arises purely due to spatial dispersion effects.

Finally, the third relation of Eq. (14) satisfies the constraints $d_y = 0$, $d_x = d_z$, i.e., the mode described by this equation is longitudinal. If $k_x = \pi$, G_k^{xz} vanishes and the latter two equations coincide, i.e., two dispersion curves touch each other at the edge of Brillouin zone.

Note that in the present analysis we assume that the scatterers are lossless. This assumption simplifies the study in general and the demonstration of spatial-dispersion-induced

birefringence in the system in particular. However, as it is proved in Sec. V below, the effect is still present in the dissipative case. The methods of investigation of the complex band structure of lossy photonic crystals and metamaterials are presented, e.g., in Refs. [32,33].

IV. ISOFREQUENCY CONTOURS

In order to study the structure dispersion properties better, we plot the system of isofrequency contours for the different frequencies. The analysis of the dispersion diagram Fig. 2 reveals the main dispersion regimes possible in the structure. The boundaries of different dispersion regimes ω_i are $\omega(A_i)$ with the points A_i depicted in Fig. 2:

(1) When $0 < \omega < \omega_1$, $\omega_1/\omega_0 \approx 0.650$ (ω_0 corresponds to the plasmonic resonance of the individual particle), the circular isofrequency contours corresponding to the two transverse eigenmodes are observed; the dispersion properties of these eigenmodes are almost the same [Fig. 3(a)].

(2) When $\omega_1 < \omega < \omega_2$, $\omega_2/\omega_0 \approx 0.690$, the differences between the two transverse polarizations become distinct. The isofrequency contours of the waves polarized along the y axis acquire the quasihyperbolic fragments whereas the dispersion regime for the other transverse polarization remains elliptic [Fig. 3(b)].

(3) When $\omega_2 < \omega < \omega_3$, $\omega_3/\omega_0 \approx 0.722$, the isofrequency contours for the waves polarized along the y axis have the shape similar to two concentric circles, and the isofrequency contours for transverse waves polarized in plane Oxz combine closed and opened (hyperbolic) fragments, the hyperbolic fragments being oriented along the coordinate axes [Fig. 3(c)].

(4) When $\omega_3 < \omega < \omega_5$, $\omega_5/\omega_0 \approx 1.382$, a stopband for the waves polarized along the y axis is observed, whereas the structure supports propagation of “longitudinal” modes as well as “transverse” eigenmodes polarized in the Oxz plane. These eigenmodes have a quasihyperbolic law of dispersion. The division of the eigenmodes into “longitudinal” and “transverse” in this frequency region is artificial to some extent. Here, the wave is classified as “longitudinal” if the angle between the local electric field and the wave vector is smaller than 45° ; otherwise the wave is classified as “transverse” [Fig. 3(d)]. But the division of eigenmodes into transverse and longitudinal is still valid for the ΓK direction of propagation (see Sec. III). If $\omega < \omega_4$ ($\omega_4/\omega_0 \approx 1.137$), the eigenmode propagating in the ΓK direction is transverse and polarized in plane Oxz ; if $\omega > \omega_4$, the eigenmode is longitudinal.

(5) When $\omega_5 < \omega < \omega_6$, $\omega_6/\omega_0 \approx 1.433$, both transverse modes are allowed to propagate in the structure. The dispersion regime for them is elliptic and the dispersion properties are almost the same. The longitudinal mode with the hyperbolic law of dispersion also exists [Fig. 3(e)].

(6) When $\omega > \omega_6$, the circular isofrequency contours for both transverse polarizations are observed; the laws of dispersion for the transverse eigenmodes are almost the same [Fig. 3(f)].

The performed analysis suggests that the polarization of eigenmodes is neither purely transverse, nor purely longitudinal in the general case. To illustrate this, we consider the propagation of the wave in the direction $(\cos \varphi, 0, \sin \varphi)$, where $\varphi = 30^\circ$. The dispersion diagram and the angle between the

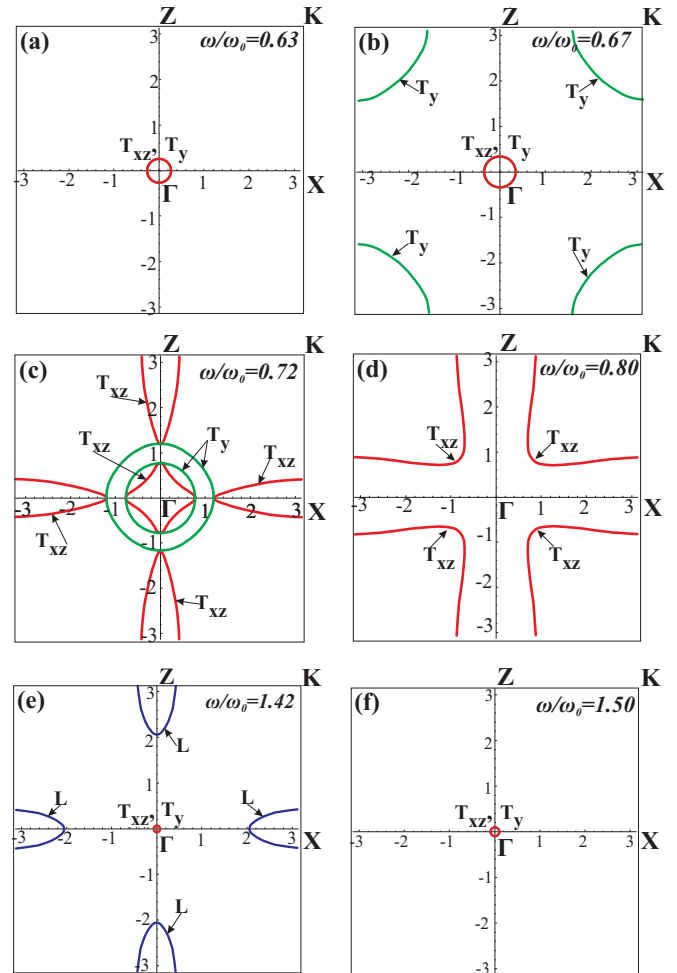


FIG. 3. (Color online) The typical isofrequency contours for the cubic lattice of isotropic particles with electric polarizability. $k_y = 0$. T_{xz} , T_y , and L mark isofrequency contours corresponding to the transverse waves with polarization in the plane Oxz , transverse waves polarized along the y axis, and longitudinal waves, respectively.

wave vector and the local electric field as the function of k_x are plotted in Fig. 4.

Our analysis demonstrates also that in the spectral region $\omega < \omega_1$ or $\omega > \omega_6$ the structure behaves as isotropic, and the effective medium model is valid. However, the unusual physical effects arise in the intermediate region $\omega_1 < \omega < \omega_6$ due to spatial dispersion. Possible experimental detection of these unusual features is specified below.

V. POSSIBLE OBSERVATION OF SPATIAL-DISPERSION-INDUCED BIREFRINGENCE IN METAMATERIALS

The results of Secs. III and IV suggest that the structure composed of isotropic particles located in the sites of a cubic lattice acquires noticeable anisotropic properties at the frequencies near the individual particle resonance. Below, we demonstrate that this spatial-dispersion-induced birefringence in metamaterials can be detected experimentally by measuring the reflection coefficients for different polarizations of the incident wave. In this section, we propose a specific scheme

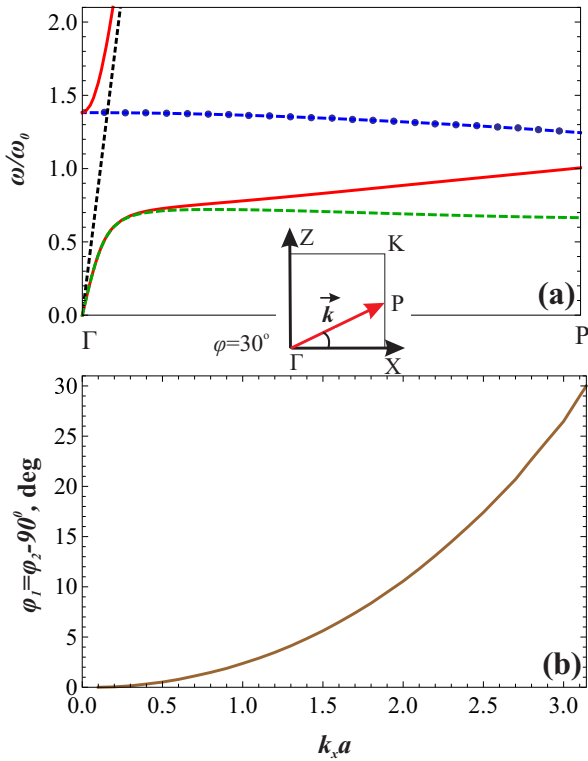


FIG. 4. (Color online) (a) The dispersion diagram for the direction of propagation $(\cos \varphi, 0, \sin \varphi)$, $\varphi = 30^\circ$. Solid curve corresponds to the “transverse” wave polarized in the plane Oxz (the angle between the electric field and the wave vector is greater than 45°); dashed curve corresponds to the transverse wave polarized along the y axis, and the dot-dashed curve corresponds to the “longitudinal” mode (the angle between the electric field and the wave vector is smaller than 45°). (b) The angle φ_1 between the local electric field and the wave vector for the “longitudinal” wave, that coincides with the angle $\varphi_2 - 90^\circ$ for the “transverse” wave.

allowing one to observe the effect (Fig. 5) and perform the calculations illustrating the effect.

We assume that the boundary of material is parallel to the crystallographic plane $(0, 1, 1)$ and study the normal incidence of the wave at the metamaterial slab [Fig. 5(a)] calculating the reflection coefficients for two linear polarizations of the impinging wave.

First we consider the effective medium approach to the formulated problem. In this approach, the structure is described by local isotropic permittivity tensor defined according to the Clausius-Mossotti formula Eq. (8):

$$\varepsilon = \frac{1 + 8\pi\alpha_0/(3a^3)}{1 - 4\pi\alpha_0/(3a^3)}, \quad (15)$$

where the polarizability of the particle is determined by Eq. (11). The reflection coefficient from the slab of isotropic dielectric is determined by the standard formula [29]. It is important that the effective medium model predicts the same reflection coefficients for both polarizations x and y of the impinging wave [Fig. 5(a)].

On the other hand, the equality $R_x = R_y$ is not required by the structure symmetry [Fig. 5(b)]. Thus, the difference

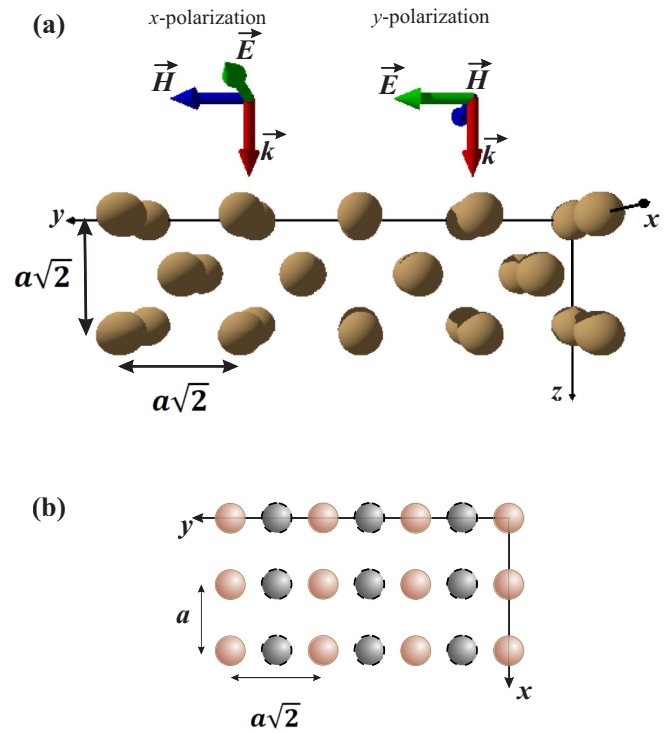


FIG. 5. (Color online) (a) A scheme of experiment allowing one to detect the anisotropy of metamaterial due to spatial dispersion by measuring the reflection coefficients for x and y polarizations of the incident wave. (b) Top view of the two upper layers of particles. Top particles are shown by solid line; bottom ones are shown by dashed contour. The choice of coordinate axes is different from that used in the previous sections.

between the reflection coefficients will provide the direct evidence of the structure anisotropy.

To describe the effect of spatial-dispersion-induced birefringence theoretically, we employ the discrete dipole model. This model is capable of capturing the difference between reflection coefficients for x - and y -polarized incident waves. We perform numerical calculations for the metamaterial slab consisting of $N = 21$ layer of spherical particles with the radius $R = a/3.6$. Permittivity of the particle material is described by the Drude model,

$$\varepsilon_p(\omega) = 1 - \frac{\omega_p^2}{\omega^2 + i\omega_c\omega}, \quad (16)$$

with the plasma frequency $\omega_p = \omega_0 \sqrt{3} = 0.229 c/a$, the resonance frequency $\omega_0 = 0.132 c/a$, and the collision frequency $\omega_c = 2.29 \cdot 10^{-3} c/a$. In order to avoid problems with the applicability of the Drude fit Eq. (16) to real materials [34,35] the described model system is investigated. This model system is scalable to arbitrary sizes and wavelengths (if the resonance frequency of the particles is also scaled). The realistic prototypes corresponding to these model parameters would be silver particles in the visible or silicon carbide particles with shells of silver in the visible [16]. The lattice period in the former case would be $a = 12$ nm, and the particle radius $R = 3.33$ nm. The calculated reflection coefficients are presented in Fig. 6(a).

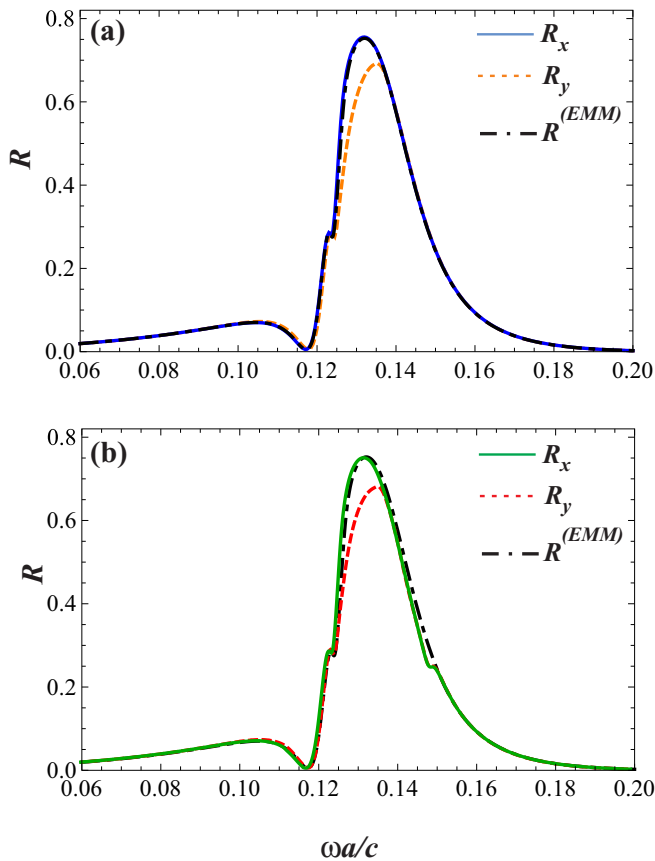


FIG. 6. (Color online) Calculated reflection coefficients for different polarizations of the incident wave: solid curve for x polarization; dashed curve for y polarization in the geometry of Fig. 5(a); dot-dashed curve shows the result derived from the local effective medium model, the same for both polarizations. (a) Discrete dipole model. (b) CST MICROWAVE STUDIO.

The details of the discrete dipole model for this problem are specified in Appendix B.

We also compare the theoretical results with ones simulated in CST MICROWAVE STUDIO for the same system [Fig. 6(b)]. In numerical simulation, the lattice period was chosen to be $a = 12$ nm and the material of the particles was defined exactly by Eq. (16). The results obtained by these two independent approaches are in very good agreement; the typical divergence between them is less than 1%. Comparing the calculated curves one can easily detect resonances due to higher-order multipoles that are not taken into account in the discrete dipole model. Namely, such a resonance exists at frequency $\omega_r = 0.148 c/a$ in the investigated system. At this frequency, the discrepancy between the two approaches is maximal and reaches 14%. Note also that the prediction of the effective medium model is in good agreement with the value of the reflection coefficient for x polarization of the incident wave, i.e., for the wave polarization along the optical axis of the crystal.

Thus, numerical simulation confirms the drawn conclusion about the difference between the reflection coefficients for the two polarizations of the incident wave. This verifies the phenomenon of spatial-dispersion-induced birefringence that can be observed in the vicinity of the individual particle

resonance even in the presence of losses. For the considered system, the difference between the reflection coefficients for two polarizations can be as large as 16% ($\omega \approx \omega_0$), and the spectral range where the difference between the two reflection coefficients is greater than 5% is $0.125 < \omega a/c < 0.135$.

Importantly, the analogous birefringence effects can be observed in transmission. The difference between transmission coefficients for x - and y -polarized waves is maximal in the vicinity of the individual particle resonance. For example, for a metamaterial slab consisting of five layers of particles with the parameters defined above, transmission coefficients are $T_x = 0.46$, $T_y = 0.28$ at the frequency $\omega = 0.131 c/a$, and thus the difference between transmission coefficients reaches 39%. Such measurements should be performed for sufficiently thin metamaterial slabs. In the case of thick slabs (more than 15 layers), transmission for both polarizations would be negligible near the resonance frequency.

It should be mentioned that some qualitative conclusions about the reflection coefficients can be drawn basing on the isofrequency contours of the structure without any additional calculations. Namely, in the vicinity of the individual particle resonance isofrequency contours have the shape of Fig. 3(d). In the geometry of Fig. 5, this means that the structure supports propagation of the y -polarized eigenmode whereas the x -polarized eigenmode is evanescent [Fig. 7(a)]. On this ground, one may expect that the reflection coefficient R_x would be *higher* than R_y in the vicinity of the particle resonance (see Fig. 6). Additionally, the proposed explanation suggests that the difference between the reflection coefficients can be detected even if the structure is semi-infinite. Therefore, the discussed anisotropy should be associated with the bulk properties of the system (i.e., its nonlocal permittivity tensor) rather than with the metamaterial surface.

Furthermore, the anisotropy of the structure can be detected regardless of the way the boundary of the metamaterial is cut. Figure 7(b) illustrates the case when the boundary is cut along the $(0,0,1)$ plane. The structure still supports the propagation of the TM mode, and the TE mode is evanescent. On the other hand, an isotropic medium equally supports propagation of the modes with both polarizations. Therefore, the relation between the reflection coefficients for TM and TE polarizations in the

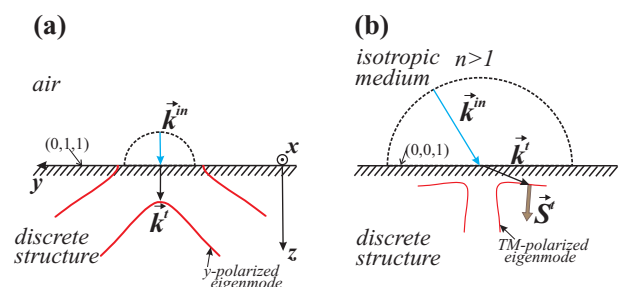


FIG. 7. (Color online) (a) Illustration of the experiment in Fig. 5 in terms of isofrequency contours. Structure supports propagation of y -polarized eigenmode whereas x -polarized mode is evanescent. (b) The boundary of the structure is cut along the $(0,0,1)$ plane. Reflection at oblique incidence reveals the birefringence effect. \vec{k} and \vec{S} denote wave vector and Poynting vector, respectively.

case of oblique incidence will not correspond to that predicted by the Fresnel's formulas.

Finally, it should be stressed that spatial dispersion effects occur in the studied system even though it is deeply subwavelength (see, e.g., axes of abscisses in Fig. 6). The intrinsic reason giving rise to the nonlocal effects is inhomogeneous field distribution over the unit metamaterial cell. As a result, local and averaged fields differ significantly. For that reason, the relation between the averaged polarization and the averaged field in the structure turns out to be essentially nonlocal although the material of inclusions is local.

VI. CONCLUSIONS

In the present work, we consider the three-dimensional metamaterial realized as an array of isotropic particles possessing electric polarizability located in the sites of a cubic lattice. We study the dispersion properties of the structure and describe spatial dispersion effects employing the discrete dipole model. The phenomenon of spatial-dispersion-induced birefringence in this metamaterial is investigated and a simple experiment allowing one to observe the effect is suggested. Namely, we propose to measure the reflection coefficients for two different polarizations of the incident wave. The difference between these reflection coefficients would be the evidence of the structure anisotropy and can be as large as 16% (for the investigated numerical example). The similar effects can be observed in transmission. We also demonstrate that the eigenmodes of the structure are neither transverse nor longitudinal but have a "mixed" polarization state in the general case.

ACKNOWLEDGMENTS

The authors acknowledge fruitful discussions with A.N. Poddubny. This work was supported by the Government of the Russian Federation (Grant No. 074-U01), "Dynasty" foundation, grant of the President of the Russian Federation MD-6805.2013.2, SPIE Optics and Photonics Education Scholarship, the Ministry of Education and Science of the Russian Federation (Projects No. 14.584.21.0009 10, GZ No. 2014/190, GZ No. 3.561.2014/K), Russian Foundation for Basic Research, Government of Saint Petersburg, and the Ministry of Education of the Republic of Belarus (Grant No. 625/02).

APPENDIX A: CALCULATION OF THE TENSOR $\hat{G}_{\vec{k}}$ COMPONENTS

The calculation of the diagonal term $G_{\vec{k}}^{xx}$ was discussed in Ref. [3]; see the final formula (A37). Note that Ref. [3] uses different designations. To obtain the result in our notations, one has to take the complex conjugate of Eq. (A37), multiply it by 4π , replace \vec{q} by \vec{k} , and k by q .

Now we proceed to the calculation of the sum $G_{\vec{k}}^{xy}$ using the Poisson summation formula and the fact that $G^{xy}(\vec{r}) = \frac{\partial^2}{\partial x \partial y} \left(\frac{e^{iqr}}{r} \right)$. We also make use of the fact that $G^{xy}(\vec{r}) = 0$ when

$x = 0$ or $y = 0$. Thus,

$$\begin{aligned} G_{\vec{k}}^{xy} &\equiv \sum_{(m,n,l) \neq (0,0,0)} G^{xy}(\vec{r}_{mnl}) e^{-i\vec{k} \cdot \vec{r}_{mnl}} \\ &= \sum_{m \neq 0} \sum_{n,l=-\infty}^{\infty} \frac{\partial^2}{\partial x \partial y} \left(\frac{e^{iqr}}{r} \right) \Big|_{r=r_{mnl}} e^{-ik_x m a - ik_y n a - ik_z l a} \\ &= \sum_{m \neq 0} \frac{\partial}{\partial x} \left\{ \sum_{n,l=-\infty}^{\infty} \frac{\partial}{\partial y} \left(\frac{e^{iqr}}{r} \right) e^{-ik_y y - ik_z z} \right\} \Big|_{r=r_{0nl}} e^{-ik_x m a} \\ &= \sum_{m \neq 0} \frac{\partial}{\partial x} \left\{ \frac{2\pi i}{a^2} \sum_{n,l=-\infty}^{\infty} (2\pi n + k_y a) \frac{e^{-|x|f(n,l)/a}}{f(n,l)} \right\} \Big|_{x=ma} \\ &\quad \times e^{-ik_x m a}, \end{aligned} \quad (\text{A1})$$

where $f(n,l) = \sqrt{(2\pi n + k_y a)^2 + (2\pi l + k_z a)^2 - q^2 a^2}$, and the sign of the square root is chosen so that $\text{Re} \sqrt{\dots} > 0$ (we assume infinitesimal positive imaginary part in q). Finally, we derive that

$$G_{\vec{k}}^{xy} = -\frac{2\pi \sin(k_x a)}{a^3} \sum_{n,l=-\infty}^{\infty} \frac{2\pi n + k_y a}{\cosh f(n,l) - \cos(k_x a)}. \quad (\text{A2})$$

The series on the right-hand side of Eq. (A2) has a very good convergence and therefore the formula (A2) is very convenient for rapid numerical calculations. Equation (A2) suggests also that $G_{\vec{k}}^{xy}(q; 0, k_y, k_z) = G_{\vec{k}}^{xy}(q; \pi/a, k_y, k_z) = 0$. The tensor $G_{\vec{k}}^{xy}$ is symmetric with respect to the permutation of k_x and k_y due to the symmetry properties of the vacuum Green's function. Therefore, we also conclude that $G_{\vec{k}}^{xy}(q; k_x, 0, k_z) = G_{\vec{k}}^{xy}(q; k_x, \pi/a, k_z) = 0$. These facts were used in Sec. IV while studying the particular cases of propagation. The off-diagonal components $G_{\vec{k}}^{xz}$ and $G_{\vec{k}}^{yz}$ are expressed by the formulas analogous to Eq. (A2).

APPENDIX B: REFLECTION FROM A SLAB OF DISCRETE METAMATERIAL: DISCRETE DIPOLE MODEL

We denote by d_l complex amplitude of the dipole moment of the particle located in the l^{th} layer where $l = 1, 2, \dots, N$, and the layers are normal to the z axis [Fig. 5(a)]. The structure period along the x axis is a ; we also use designations $b = a\sqrt{2}$, and $c = a/\sqrt{2}$. The self-consistent equations determining the amplitudes of the dipole moments of the scatterers d_l are as follows [36]:

$$\begin{aligned} \alpha^{-1} d_l &= \sum_{l' \neq l} \beta_{l'-l} d_{l'} + \beta_0 d_l + E^{\text{in}} e^{iqc} \quad (\text{x polarization}), \\ \alpha^{-1} \tilde{d}_l &= \sum_{l' \neq l} \tilde{\beta}_{l'-l} \tilde{d}_{l'} + \tilde{\beta}_0 \tilde{d}_l + E^{\text{in}} e^{iqc} \quad (\text{y polarization}), \end{aligned} \quad (\text{B1})$$

with

$$\beta_s = \sum_{m,n=-\infty}^{\infty} G^{xx}(\vec{r}_{mns} + sc\vec{e}_z), \quad s \neq 0, \quad (\text{B2})$$

$$\tilde{\beta}_s = \sum_{m,n=-\infty}^{\infty} G^{yy}(\vec{r}_{mns} + sc\vec{e}_z), \quad s \neq 0,$$

$$\beta_0 = \sum_{(m,n) \neq (0,0)} G^{xx}(\vec{r}_{mn0}), \quad (\text{B3})$$

$$\tilde{\beta}_0 = \sum_{(m,n) \neq (0,0)} G^{yy}(\vec{r}_{mn0}),$$

where $\vec{r}_{mns} = ma\vec{e}_x + (nb + \delta_s)\vec{e}_y$, and m and n are integers. If s is a multiple of 2, $\delta_s = 0$, otherwise $\delta_s = b/2$. The expressions for β_s and $\tilde{\beta}_s$ suitable for rapid numerical calculations can be derived using the Poisson summation formula in the way similar to that in Ref. [36]:

$$\beta_s = -\frac{2\pi i}{ab} \sum_{m,n=-\infty}^{\infty} \left[\left(\frac{2\pi m}{a} \right)^2 - q^2 \right] \frac{e^{ik_{mn}^{(z)}|s|c} (-1)^{ns}}{k_{mn}^{(z)}}, \quad (\text{B4})$$

$$\tilde{\beta}_s = -\frac{2\pi i}{ab} \sum_{m,n=-\infty}^{\infty} \left[\left(\frac{2\pi n}{b} \right)^2 - q^2 \right] \frac{e^{ik_{mn}^{(z)}|s|c} (-1)^{ns}}{k_{mn}^{(z)}}, \quad (\text{B5})$$

where

$$k_{mn}^{(z)} = \sqrt{q^2 - (2\pi m/a)^2 - (2\pi n/b)^2}.$$

The sign of the square root is chosen according to the requirement $\text{Im} k_{mn}^{(z)} \geq 0$ and the infinitesimal positive imaginary part

of q is assumed. The expressions for β_0 and $\tilde{\beta}_0$ are more complicated and can be expressed via all β_s , $\tilde{\beta}_s$ with nonzero s in terms of infinite three-dimensional sums that have already been calculated in Appendix A:

$$\begin{aligned} \beta_0 &= G_k^{xx}(q; 0, 0, 0) + \frac{4\pi i}{ab} \sum_{m,n=-\infty}^{\infty} \left[\left(\frac{2\pi m}{a} \right)^2 - q^2 \right] \\ &\quad \times \frac{1}{k_{mn}^{(z)}} \frac{(-1)^n e^{-ik_{mn}^{(z)}c} + 1}{e^{-2ik_{mn}^{(z)}c} - 1}, \\ \tilde{\beta}_0 &= G_k^{yy}(q; 0, 0, 0) + \frac{4\pi i}{ab} \sum_{m,n=-\infty}^{\infty} \left[\left(\frac{2\pi n}{b} \right)^2 - q^2 \right] \\ &\quad \times \frac{1}{k_{mn}^{(z)}} \frac{(-1)^n e^{-ik_{mn}^{(z)}c} + 1}{e^{-2ik_{mn}^{(z)}c} - 1}. \end{aligned} \quad (\text{B6})$$

Note that x and y axes that appear in matrix elements G_k^{xx} and G_k^{yy} correspond to the geometry of Fig. 5. The terms of the series (B4)–(B6) that correspond to $m = n = 0$ describe the field of the plane with a continuous polarization distribution. It is this term that is responsible for the far field radiated by the metamaterial slab. Once the coefficients β_s and $\tilde{\beta}_s$ are calculated, the linear system Eq. (B1) can be solved with respect to d_l or \tilde{d}_l . Considering the reflected field at sufficiently large distances from the metamaterial slab we calculate the reflection coefficient as follows:

$$\begin{aligned} R &= \left| \frac{2\pi q}{ab E^{\text{in}}} \right|^2 \left| \sum_{l=1}^N d_l e^{iq_l c} \right|^2 \quad (x \text{ polarization}), \\ \tilde{R} &= \left| \frac{2\pi q}{ab E^{\text{in}}} \right|^2 \left| \sum_{l=1}^N \tilde{d}_l e^{iq_l c} \right|^2 \quad (y \text{ polarization}). \end{aligned} \quad (\text{B7})$$

-
- [1] I. Bloch, *Nature Phys.* **1**, 23 (2005).
[2] E. L. Ivchenko, Y. Fu, and M. Willander, *Phys. Solid State* **42**, 1756 (2000).
[3] P. A. Belov and C. R. Simovski, *Phys. Rev. E* **72**, 026615 (2005).
[4] M. G. Silveirinha, *Phys. Rev. B* **76**, 245117 (2007).
[5] M. A. Gorlach and P. A. Belov, *Phys. Rev. B* **90**, 115136 (2014).
[6] P. A. Belov, R. Marques, S. I. Maslovski, I. S. Nefedov, M. Silveirinha, C. R. Simovski, and S. A. Tretyakov, *Phys. Rev. B* **67**, 113103 (2003).
[7] M. G. Silveirinha and P. A. Belov, *Phys. Rev. B* **77**, 233104 (2008).
[8] C. R. Simovski, P. A. Belov, A. V. Atrashchenko, and Y. S. Kivshar, *Adv. Mater.* **24**, 4229 (2012).
[9] R. E. Collin, *Field Theory of Guided Waves* (IEEE Press, New York/Piscataway, 1991).
[10] D. V. van Coevorden, R. Sprik, A. Tip, and A. Lagendijk, *Phys. Rev. Lett.* **77**, 2412 (1996).
[11] R. A. Shore and A. D. Yaghjian, *Radio Sci.* **42**, 003647 (2007).
[12] R. A. Shore and A. D. Yaghjian, *Radio Sci.* **43**, 003814 (2008).
[13] R. A. Shore and A. D. Yaghjian, *Radio Sci.* **47**, 004859 (2012).
[14] R. A. Shore and A. D. Yaghjian, *Radio Sci.* **47**, 004860 (2012).
[15] S. Campione, M. B. Sinclair, and F. Capolino, *Photonics and Nanostructures—Fundamentals and Applications* **11**, 423 (2013).
[16] A. Alu and N. Engheta, *Phys. Rev. B* **75**, 024304 (2007).
[17] V. L. Ginzburg, *J. Exp. Theor. Phys.* (in Russian) **34**, 1593 (1958).
[18] V. M. Agranovich and V. L. Ginzburg, *Spatial Dispersion in Crystal Optics and the Theory of Excitons* (Wiley-Interscience, New York, 1966).
[19] E. F. Gross and A. A. Kaplanskiy, Reports of the USSR Academy of Sciences (in Russian) **132**, 98 (1960).
[20] E. F. Gross and A. A. Kaplanskiy, Reports of the USSR Academy of Sciences (in Russian) **139**, 75 (1961).
[21] J. H. Burnett, Z. H. Levine, and E. L. Shirley, *Phys. Rev. B* **64**, 241102 (2001).
[22] J. H. Burnett, Z. H. Levine, E. L. Shirley, and J. H. Bruning, *J. Nanolithography* **1**, 213 (2002).
[23] M. G. Silveirinha, *Phys. Rev. B* **75**, 115104 (2007).
[24] E. M. Purcell and C. R. Pennypacker, *Astrophys. J.* **186**, 705 (1973).
[25] B. T. Draine, *Astrophys. J.* **333**, 848 (1988).

- [26] P. de Vries, D. V. van Coevorden, and A. Lagendijk, *Rev. Mod. Phys.* **70**, 447 (1998).
- [27] M. A. Gorlach, A. N. Poddubny, and P. A. Belov, *Phys. Rev. B* **90**, 035106 (2014).
- [28] A. Alu, *Phys. Rev. B* **84**, 075153 (2011).
- [29] M. Born and E. Wolf, *Principles of Optics*, 4th ed. (Pergamon Press, Oxford, 1965).
- [30] L. D. Landau and E. M. Lifshitz, *Electrodynamics of Continuous Media* (Pergamon Press, Oxford, 1984).
- [31] J. E. Sipe and J. van Kranendonk, *Phys. Rev. A* **9**, 1806 (1974).
- [32] V. Kuzmiak and A. A. Maradudin, *Phys. Rev. B* **58**, 7230 (1998).
- [33] A. Orlov, I. Iorsh, P. Belov, and Y. Kivshar, *Opt. Exp.* **21**, 1593 (2013).
- [34] M. A. Ordal, L. L. Long, R. J. Bell, S. E. Bell, R. R. Bell, R. E. Alexander, J. A. Ward, and C. A. Ward, *Appl. Opt.* **22**, 1099 (1983).
- [35] A. D. Rakic, A. B. Djuricic, J. M. Elazar, and M. L. Majewski, *Appl. Opt.* **37**, 5271 (1998).
- [36] P. A. Belov and C. R. Simovski, *Phys. Rev. B* **73**, 045102 (2006).